HHS Public Access

Author manuscript

Nat Chem Biol. Author manuscript; available in PMC 2021 March 14.

Published in final edited form as:

Nat Chem Biol. 2020 December ; 16(12): 1368–1375. doi:10.1038/s41589-020-0646-2.

Sterols in an intramolecular channel of Smoothened mediate Hedgehog signaling

Xiaofeng Qi[1], **Lucas Friedberg**[1], **Ryan DeBose-Boyd**[1], **Tao Long**[1], **Xiaochun Li**[1,2,*]

[1]Department of Molecular Genetics, University of Texas Southwestern Medical Center, Dallas, TX 75390, USA

[2]Department of Biophysics, University of Texas Southwestern Medical Center, Dallas, TX 75390, USA

Abstract

Smoothened (SMO), a class-Frizzled G protein-coupled receptor (class-F GPCR), transduces the Hedgehog signal across cell membrane. Sterols can bind to its extracellular cysteine rich domain (CRD) and to several sites in the 7 transmembrane helices (7-TMs) of SMO. However, the mechanism how sterols regulate SMO via multiple sites is unknown. Here we determined structures of SMO–G_i complexes bound to the synthetic SMO agonist (SAG) and to 24(*S*),25-epoxycholesterol (24(*S*),25-EC). A novel sterol-binding site in the extracellular extension of TM6 was revealed to connect other sites in 7-TMs and CRD, forming an intramolecular sterol channel from the middle side of 7-TMs to CRD. Additional structures of two gain-of-function variants, SMO^{D384R} and $SMO^{G111C/I496C}$, showed that blocking the channel at its midpoints allows sterols to occupy the binding sites in 7-TMs, thereby activating SMO. These data indicate that sterol transport through the core of SMO is a major regulator of SMO-mediated signaling.

Introduction

Hedgehog is a secreted protein that is essential for normal development, and it is also implicated in various cancers [1–4]. Hedgehog binds PTCH1 to disrupt the sterol tunnel in PTCH1 [5–9] and triggers the internalization of PTCH1 [10], leading to sterol accumulation on the cell surface. Subsequently, SMO redistributes on the cell surface to sense the accumulating sterols that serve as its endogenous agonists, resulting in activation of the

*Correspondence should be addressed to X.L. (xiaochun.li@utsouthwestern.edu).

Authors Contributions

X.L. conceived the project and designed the research with X.Q. X.Q. purified the protein for cryo-EM study and performed the functional characterization with L.F., R.D.B. and T.L. X.Q. carried out cryo-EM work, built the model, refined the structure. X.Q. and T.L. and X.L. analyzed the data. All the authors contributed to manuscript preparation and X.L. wrote the manuscript.

Competing interests The authors declare no competing financial interests.

Data Availability Statement: The data that support the findings of this study are available from the corresponding author upon request. The 3D cryo-EM density maps have been deposited in the Electron Microscopy Data Bank under the accession number EMD-22119, EMD-22120, EMD-22117 and EMD-22118. Atomic coordinates for the atomic model have been deposited in the Protein Data Bank under the accession number 6XBL, 6XBM, 6XBJ and 6XBK.

Glioma-associated oncogene (GLI) transcription factors that promote cell proliferation and differentiation [11].

SMO is a member of the class-F GPCR superfamily and comprises an N-terminal extracellular CRD [12,13], an extracellular linker domain (LD) that leads to the 7-TMs, and a C-terminal cytosolic tail with over 200 residues (Extended Data Fig. 1). As a member of GPCRs, the 7-TMs of SMO have been shown to accommodate numerous synthetic SMO compounds including agonists (e.g. SAG) and antagonists (e.g. Vismodegib, SANT1 and LY2940680) [14–16]. Previous studies have shown that a sterol molecule can bind either in the 7-TMs or the CRD of SMO to trigger its activation [13–15,17–20]. Mutations in either the 7-TMs or the CRD that interfere with sterol binding abolish signaling directly, suggesting that both binding sites are essential for Hedgehog signaling [15,19,21]. The CRD represses the activity of SMO; notably, previous studies have shown that this repression can be removed when the CRD is deleted or bound by a sterol [12,22].

Although a framework for SMO interactions with natural or synthetic ligands has recently been provided by X-ray crystallography [13,15,17,19,23] and cryo-EM studies [14], the presence of multiple binding sites, and the functional relationship among these sites is still unknown. The current study was undertaken to search for a functional relationship between these sites. The results demonstrate that the cholesterol binding sites are arrayed along a continuous channel through SMO; and blocking this channel to keep cholesterol in the 7-TMs can introduce constitutive Hedgehog signaling.

Results

SAG blocks an endogenous sterol in the 7-TMs

Previous structural studies have used a C-terminally truncated SMO protein [14,15,17,19,23] because the C-terminal flexible tail of SMO negatively affects the protein's behavior; however, this tail is required for SMO trafficking from the cytosol to the cell surface [24,25]. Therefore, we screened human SMO (hSMO) constructs with different C-terminal truncations. The GLI-dependent luciferase assay showed that the variant comprising residues 1–644 is the shortest construct that retains activity in $Smo^{-/-}$ MEF cells (Extended Data Fig. 1), supporting another study that mouse SMO^{1-637} (mSMO, residues 1–637) retains Hedgehog response activity in $Smo^{-/-}$ MEFs [25]. Therefore, we used $hSMO^{1-644}$ for our structural investigations. Previous studies have shown that active SMO can recruit heterotrimeric G_i [14,26,27]; moreover, the physiological role of G_i has been shown in noncanonical Hedgehog signaling [28]. In this study, we used G_i proteins as SMO effectors that facilitate the capture of an active conformation of SMO by cryo-EM.

We have previously shown that SAG can stimulate SMO to recruit heterotrimeric G_i [14]. To study SAG function in SMO activation in atomic detail, a hSMO complex with G_i and the single-chain variable fragment scFv16 [29] was assembled in the presence of SAG. The structure of this complex was determined at 3.96-Å resolution (Fig. 1a, Extended Data Fig. 2a, Supplementary Figures 1, 2 and Supplementary Table 1), revealing an assembly similar to the previously reported structure of the SMO–G_i–24(S),25-EC complex [14] (Extended Data Fig. 3a). Compared to inactive SMO structures, TM5 and TM6 of hSMO show 4–5-Å

shifts, suggesting that SAG-bound hSMO is representative of the active conformation (Extended Data Fig. 3b). The residues 539–644 were not observed in the cryo-EM map, suggesting high flexibility of this region. This tail may become structured upon binding to other proteins [30].

Although the overall map of CRD was poorly defined, the two major helices of the CRD were observed in the cryo-EM map (Extended Data Fig. 2a and Supplementary Figure 2). Since the CRD is rigid and stabilized by several disulfide bonds as observed in previous structures [12,20], we docked a crystal structure of CRD into the map as a rigid body based on map of its major helices (Fig. 1a). Unlike in previously determined snapshots of the CRD in the active SMO, which were stabilized by crystal packing [15,17], the orientation of the CRD in the cryo-EM map presumably represents an average of active states in solution. The CRD conformation most closely resembles the mSMO–SAG21k–nanobody complex [15] (Fig. 1c).

Remarkably, a strong sterol-like density adjacent to the SAG density was found in the 7-TMs, which we refer to as “site 1” for the remainder of the text (Fig. 1a, b). The residues in the 7-TMs create a hydrophobic pocket to accommodate the sterol (Fig. 1d). A cholesterol, representative of sterol, is modeled in this site. The position of this endogenous cholesterol is consistent with the deep sterol-binding site in the crystal structure of the mSMO–SAG21k–nanobody complex [15] (Fig. 1e). The sterol in this crystal structure most likely originated from the lipidic mesophase that contained 10% cholesterol [15]. By contrast, no cholesterol or its derivatives was supplemented during the preparation of the SMO–G_i–SAG complex here, indicating that an endogenous cholesterol was bound to the 7-TMs. If the 4-aminomethyl group of SAG was elongated [31], it would sterically interfere with binding of an endogenous cholesterol in the 7-TMs (Fig. 1e), explaining why SAG can be converted into an antagonist by a substitution of its 4-aminomethyl group with larger aliphatic groups [31]. Indeed, bona-fide synthetic antagonists of SMO (e.g. Vismodegib, SANT-1, and LY2940680) compromise binding of an endogenous cholesterol (Fig. 1f), thereby abolishing signaling.

24(*S*),25-EC can bind SMO at a novel site

24(*S*),25-EC is an oxysterol that triggers the Hedgehog [14,32] and G protein signal [14] via SMO. We have used 24(*S*),25-EC as a cholesterol representative to study how SMO couples to G_i proteins by determining the structure of the SMO–G_i–24(*S*),25-EC complex at 4.0 Å resolution [14]. Owing to the limited resolution, we did not obtain enough information for sterol-mediated SMO activation. We therefore assembled a SMO–G_i complex with scFv16 in the presence of 24(*S*),25-EC. The structure was determined at 3.14 Å resolution (Fig. 2a, Extended Data Fig. 2b, Supplementary Figures 3, 4 and Supplementary Table 1). Due to the heterogenous resolution distribution, the resolution of the receptor is lower than that of trimeric G protein (Supplementary Figure 4b). In the membrane region, a strong sterol-like density was observed in the upper sterol-binding site (referred to as “site 2”) after 3D auto-refinement by RELION-3 (Fig. 2a and Extended Data Fig. 3c), as previously reported [14] . Notably, at a lower threshold level in the auto-refined map or after postprocessing by RELION-3, this density was elongated to the bottom of site 1 (the orange maps in Fig. 2a). At a higher threshold level of 0.0184, the elongated density in the postprocessed map

disappears and the rest of the map is consistent with the map after 3D auto-refinement (the green maps in Fig. 2a), suggesting some flexibility of this part in site 1. As the density in site 2 is still visible, we modeled it as 24(*S*),25-EC (Fig. 2b). It is possible that the 24(*S*),25-EC binds both sites and that the elongated density represents an average of 24(*S*),25-EC occupying various locations along this channel. Residue N219 may bind the hydroxyl group of the 24(*S*),25-EC in site 2 (Fig. 2c).

Intriguingly, another sterol-like molecule was observed between the extracellular extension of TM6 and the LD (referred to as "site 3") (Fig. 2a and Extended Data Fig. 2b). Residue Y207 of the LD blocks the sterol in site 3 (Fig. 2c). Site 3 is farther from the membrane than any other binding site in the 7-TMs of SMO (Figs. 1f and 2b, c). Structural comparison between 24(*S*),25-EC-bound and SAG-bound SMO shows a 6-Å movement on the extracellular region of TM6, due to residues F484, R485 and V488 of TM6 involvement in 24(*S*),25-EC binding (Fig. 2c, d). In this complex, the density of the CRD is ambiguous, consistent with our previous structural observation [14]. Structural studies have revealed that the CRD can bind cholesterol, 20(*S*)-hydroxycholesterol, and cyclopamine [13,18,33]. We speculate that the CRD can also accommodate 24(*S*),25-EC. *Xenopus laevis* SMO–CRD (xCRD) shares 80% sequence similarity with hSMO-CRD and the cholesterol binding residues are highly conserved (Extended Data Fig. 4). Therefore, xCRD was purified from *E. coli* as previously reported [13] and used for the sterol binding assay. The result shows that xCRD can bind to cholesterol-conjugated beads and that this binding can be abolished by adding 100μM 24(*S*),25-EC (Extended Data Fig. 5). Therefore, we named this site in the CRD "site 4".

In the SAG-bound state, TM6 blocks site 3 preventing cholesterol access to site 4 (Fig. 2e). When 24(*S*),25-EC binds to site 3, it triggers a conformational change of TM6 allowing sites 3 and 4 to align, facilitating 24(*S*),25-EC's entrance into site 4 (Fig. 2e). It is possible that the CRD captures 24(*S*),25-EC during the purification. 24(*S*),25-EC binding in site 4 introduces multiple conformations of the CRD, resulting in a weak density after 3D classification (Supplementary Figure 3). In fact, the CRD orientations in two active SMO structures differ by a 120° rotation [15,17] (Fig. 1c), indicating potentially different conformations of CRD in active SMO.

Two gain-of-function SMO variants trap sterols in 7-TMs

Our structures combined with previous studies revealed four sterol binding sites in SMO (Fig. 2b, e). Since 24(*S*), 25-EC has been supplemented during the entire purification process, the structure of 24(*S*), 25-EC bound SMO may be a representative of SMO in a high sterol level environment. Moreover, functional and structural studies have shown that many agonists bind to different sites enabling the activation of SMO: 20(*S*)-hydroxyl cholesterol binds to CRD [12], SAG binds to 7-TMs, 24(*S*), 25-EC and cholesterol bind to both the CRD and the 7-TMs [15]. We hypothesize that cholesterol binding to the 7-TMs is physiologically important in SMO activity and that agonists bound to the extracellular regions facilitate cholesterol entrapment in the 7-TMs for SMO activation. Therefore, we generated a series of mutants on the residues between site 1 and site 3, attempting to trap the cholesterol in site 1 or 2. Based on our hypothesis, gain-of-function SMO variants without

any supplemented agonist may further illuminate the role of endogenous cholesterol in SMO activation. Two SMO variants were detected to be constitutively active via cell based HH signaling assay (Fig. 3a).

First, we generated a SMO^{D384R} variant that creates steric hindrance to restrict an endogenous sterol to site 1. The GLI-dependent luciferase assays show that this mutant can induce a constitutively active Hedgehog signal without SAG stimulation, similar to the previously reported gain-of-function mutant SMO^{D473R} [34] (Fig. 3b, c). It is quite possible that D473R and D384R may share a similar mechanism since they are located in the same level of the intramolecular channel of SMO and face each other. The western blotting shows that the expression level of SMO^{D384R} is similar to wild type SMO (Extended Data Fig. 6). The measurement of the mRNA level of GLI shows that, like SMO^{D473R}, the mRNA in SMO^{D384R} are 2–3-fold higher than that in wild type. Interestingly, after we depleted sterol levels in cells by adding hydroxypropyl-β-cyclodextrin (HPCD), the mRNA level of GLI in SMO^{D384R}, as well as in wild type SMO, decreased rapidly (Fig. 3d). This assay supports the notion that SMO^{D384R} can trap sterol in the 7-TMs to trigger the Hedgehog signal and the trapped sterol in site 1 can be depleted by HPCD.

We further disrupted the sterol binding site of the 7-TMs by introducing a loss-of-function mutation V329F [15,19]. The structural comparison of inactive SMO^{V329F} [19] with wild type shows no conformational changes in the 7-TMs, suggesting that V329F does not interfere with protein folding (Extended Data Fig. 7a). It also suggests that V329F may disrupt the endogenous cholesterol binding in the 7-TMs (Extended Data Fig. 7b). The cell signaling assays showed that the V329F mutation abolishes the signal activity of SMO variants D384R (Fig. 3e). This finding indicates that the Hedgehog signal that was introduced by the accumulation of cholesterol in the 7-TMs can be abolished when site 1 is mutated. However, after introducing the V329F mutation, another gain-of-function variant SMO^{W535L} (M2) still retains its activity (Fig. 3e), since it leads to a dynamic activation in the intracellular regions of SMO.

The cryo-EM structure of G_i-coupled SMO^{D384R} complex was determined at 3.88-Å resolution, revealing how SMO^{D384R} holds an endogenous cholesterol in site 1 to engage G_i proteins by its intracellular regions without any synthetic agonist (Fig. 4a, b, Extended Data Fig. 2c Supplementary Figures 5, 6 and Supplementary Table 1). The density of the CRD is not as clear as SAG bound SMO, although it is quite distinguishable after 3D classification (Supplementary Figure 5). Structural comparison shows that there is no notable conformational change between the intracellular regions in SMO^{D384R}, SAG-bound SMO, and 24(*S*),25-EC-bound SMO (Fig. 4c). The extracellular region of SMO^{D384R} shares a similar conformation with SAG-bound SMO because the cholesterol has been trapped in site 1 by the D384R mutation and cannot reach site 3 to trigger the shift on the extracellular region of TM6 (Fig. 4c).

To test the role of extracellular site 3, we generated a mutant $SMO^{G111C/I496C}$ that crosslinks the CRD and TM6 by a disulfide bond and the formation of the designed disulfide bond was confirmed by mass spectrometry (Extended Data Fig. 8), presumably to shrink the space of site 3 to prevent cholesterol binding to site 3. The GLI-dependent luciferase assays show that

this mutant is constitutively active (Fig. 5a). The western blotting shows that the expression level of $SMO^{G111C/I496C}$ is similar to wild type SMO (Extended Data Fig. 6). The mRNA level of GLI in $SMO^{G111C/I496C}$ is almost 20-fold higher than that of wild type and drops ~60% after cholesterol depletion (Fig. 5b). When site 1 is abolished by the V329F mutation, the $SMO^{G111C/V329F/I496C}$ variant also loses its basal activity, supporting that $SMO^{G111C/I496C}$ variant contains cholesterol for its activation (Fig. 3e), like the SMO^{D384R} variant.

The G_i-coupled $SMO^{G111C/I496C}$ mutant was determined at 3.24-Å resolution (Fig. 5c, Extended Data Fig. 2d, Supplementary Figures 7, 8 and Supplementary Table 1). The density of major helices in the CRD is quite distinguishable (Fig. 5c) because the CRD is stabilized by the designed disulfide bond with TM6. As in the 24(*S*),25-EC-bound structure, an endogenous sterol density was observed in site 2 and extended to site 1 (Fig. 5d). A cholesterol molecule was modeled in site 2. The structural comparison shows that the engineered disulfide bond induced a 4-Å shift on the extracellular region of TM6 compared to the SAG-bound SMO structure (Fig. 5e). Notably, this disulfide bond immobilizes the CRD and induces a conformational change of the LD, leading to a shift of residue Y207 that disrupts site 3 (Fig. 5e). This observation corroborates our hypothesis that the TM6 and the LD serve as a gate to control the transfer of cholesterol within the channel between the 7-TMs and the CRD. Interference of site 3 may cause cholesterol to be trapped in the 7-TMs. It also supports a previously published finding that disrupting the disulfide bonds in site 3 (C197S/C217S in mSMO) causes a higher basal level of Hedgehog signaling [19].

Discussion

Previous structural studies showed that PTCH1 [5–7,35,36] and NPC1 [37,38] also contain a sterol tunnel through their ectodomains to the transmembrane region to serve as a cholesterol transporter. In this work, we report four SMO–G_i complexes in distinct states showing that SMO, a GPCR, also has a sterol channel for Hedgehog signal transduction. The G_i proteins in the four complexes show highly similar conformations (Extended Data Fig. 3d). By contrast, the extracellular region of TM6 and LD adopt different conformations for SMO activation (Fig. 5e), indicating a physiological role of the long extracellular extension of the TM6 and the LD that are unique among GPCRs.

Based on our discovery of an intramolecular channel in SMO (Extended Data Fig. 9), we propose a model of Hedgehog signaling transduction, where cholesterol occupancy in this channel is critical for SMO activation. PTCH1, the cell surface receptor of Hedgehog, has been shown to transport free cholesterol into the extracellular space, preventing an accumulation of free cholesterol on the cell surface membrane, specifically the primary cilium membrane for vertebrates. When PTCH1 localizes in the cilium, SMO still stays in the intracellular vesicles. There is not enough free cholesterol to occupy all sites in the channel of SMO, so cholesterol may transport through the channel to the CRD. SMO is off in this state [7,39]. When Hedgehog binds to PTCH1, internalization of PTCH1 is triggered [10] and, thus, transport activity is abolished [6]. As a result, concentration of free cholesterol would increase on the primary cilium membrane [6,7,40]. SMO accumulates in the primary

cilium where sterol is high. Elevated cholesterol levels may then occupy all sites in the intramolecular channel of SMO, activating SMO for signaling (Fig. 6).

The CRD would down-regulate the basal signaling activity of SMO by sequestering the cholesterol moving from the 7-TMs, which is supported by the observation that deletion of CRD results in a higher basal activity of SMO [12,19]. Two mutants (D99A and Y134F in mSMO, equal to D95A and Y130A in humans) can be activated by SAG, but do not respond to the sterol directly [19]. It is tempting to speculate that the CRD of these two mutants cannot bind or trap the cholesterol in the end of the channel; however, the fate of cholesterol in the extracellular space remains unknown. Since these variants have intact 7-TMs, SAG can still keep the cholesterol in the 7-TMs to trigger the signal [19]. Moreover, a previous study showed that cholesterol can covalently bind to residue D99 of mouse CRD [21] in order to induce signaling. It is conceivable that the covalent bond is a stronger stimulus than specific binding in the channel, leading to sterol entrapment in the 7-TMs.

Methods

Protein expression and purification

Human Smoothened (hSMO) with a C-terminal truncation (Δ645–787) was cloned into pEG BacMam with a C-terminal Flag tag. The protein was expressed using baculovirus-mediated transduction of mammalian HEK-293S GnTI^{-} cells (ATCC). At 60 hours post infection at 30 °C, cells were disrupted by sonication in buffer A (20 mM Hepes pH 7.5, 150 mM NaCl) with 1 mM PMSF, 10 μg/mL leupeptin. After low-speed centrifugation, the resulting supernatant was incubated in buffer A with 1% (w/v) n-Dodecyl-β-D-maltoside (DDM, Anatrace) for 1 hour at 4 °C. The lysate was centrifuged again, and the supernatant was loaded onto an Anti-Flag M2 affinity column (Sigma). After washing twice, the protein was eluted in buffer B (20 mM Hepes pH 7.5, 150 mM NaCl and 0.02% DDM) with 0.1 mg/ml FLAG peptide. After concentrated, the protein was further purified by Superose-6 size-exclusion chromatography (GE Healthcare) in buffer B. The peak fractions were collected for complex assembly. The mutated DNA constructs were generated using QuikChange II XL Site-Directed Mutagenesis Kit (Agilent). The expression and purification of hSMO variants were the same as that of wild type hSMO. For the purification of hSMO and 24(*S*),25-epoxycholesterol (24(*S*),25-EC) complex, 5 μM 24(*S*),25-EC (Abcam) was added into the cell before sonication and 1 μM 24(*S*),25-EC was added in the wash, elution and size-exclusion buffers. The expression and purification of trimeric G_i protein and scFv16 were performed based on a published method [29].

Assembly of hSMO–G_i–scFv16 complex

Generally, purified hSMO was mixed with the G_i heterotrimer at a 1:1.1 molar ratio. This mixture was incubated at 4°C for 1 hour, followed by the addition of apyrase to catalyze the hydrolysis of unbound GDP at 4°C for 1 hour. Then the mixture was diluted 10-fold by buffer C (20 mM Hepes pH 7.5, 150 mM NaCl, 0.005% (w/v) GDN (Anatrace)) and the scFv16 was added at a 1.5:1 molar ratio (scFv16: hSMO), followed by 30 minutes incubation at 4°C. To remove excess G_i and scFv16 proteins, the mixture was purified by anti-Flag M2 antibody affinity chromatography. The complex was eluted in buffer C

supplemented by 0.1 mg/ml FLAG peptide. After concentrating, the complex was further purified by size-exclusion chromatography in buffer C. Peak fractions were concentrated to ~ 6–8 mg/ml for electron microscopy studies. For hSMO–G_i–SAG complex preparation, 100 μM SAG was added into the hSMO and G_i mixture and buffer C was supplemented by 10 μM SAG. For hSMO–G_i–EC complex preparation, 24(*S*),25-EC was added into the hSMO–EC complex and G_i mixture at a final concentration of 2 μM and buffer C was supplemented by 1 μM 24(*S*),25-EC. For the preparation of $hSMO^{D384R}$–G_i and $hSMO^{G111C/I496C}$–G_i complexes, no agonist was added during the entire process.

The CRD binding assay

Azide agarose beads, alkyne cholesterol and Click-&-Go Click Chemistry Capture Kit were purchased from Click Chemistry Tools. Alkyne cholesterol was conjugated to the azide agarose beads by click reaction following the manual from the kit with minor modifications. Briefly, 250 μL azide agarose beads and 0.5 mM alkyne cholesterol were mixed in 1 mL Copper Catalyst Solution supplemented by 20% (v/v) ethanol and the click reaction was performed at room temperature for 20 hours. Then, the cholesterol-conjugated beads were washed 5 times by 20% (v/v) ethanol and stored in 20% (v/v) ethanol at 4°C for further use.

The cysteine-rich domain (CRD, residues 35–154) of *Xenopus laevis* SMO was subcloned into pET-32a for *E. coli* expression as previously reported [13]. The expression and purification were performed as previously reported [13] without removing the tags. The protein was first incubated with DMSO or 100 μM 24(*S*),25-EC at room temperature for 1 hour, followed by the addition of either the original azide agarose beads or cholesterol-conjugated beads. The mixture was incubated overnight at 4 °C for affinity capture. The beads were washed with buffer B containing DMSO or 100 μM 24(*S*),25-EC and protein loading dye was added into the beads directly to denature the protein. After spinning down briefly, the supernatant was loaded into a protein gel for western blotting using the Anti-Histidine tagged primary antibody (1:1000, Sigma-Aldrich 05–949). The experiment was repeated three times with similar results.

Validation of disulfate bonds in $SMO^{G111C/I496C}$

The $hSMO^{G111C/I496C}$ (residues 1–644) protein was incubated with water for 40 minutes; then supplemented with iodoacetamide at 150 mM final concentration at room temperature for 40 minutes and mixed with SDS-gel loading buffer for SDS-PAGE analysis. The resulting band was cropped for the mass spectrometry analysis as a negative control. The wild type hSMO and $hSMO^{G111C/I496C}$ proteins were incubated with 5 mM TCEP (Sigma-Aldrich, dissolved in water) at room temperature for 40 minutes; then supplemented with iodoacetamide at 150 mM final concentration at room temperature for additional 40 minutes incubation, and finally mixed with SDS-gel loading buffer for SDS-PAGE analysis. The resulting bands were cropped for the mass spectrometry analysis. No additional reduction or alkylation was performed during the sample preparation. The samples were digested by trypsin and analyzed by Liquid Chromatography-Mass Spectrometry (LC-MS). The data were analyzed using Proteome Discoverer 2.4 and was searched using the human protein database from Uniprot along with SMO^{WT} and $SMO^{G111C/I496C}$ sequences. The experiment was re-produced twice in the different weeks with similar results.

EM Sample Preparation and Imaging

The 6–8 mg/ml protein complexes were used for electron microscopy studies. The freshly purified hSMO–G_i complexes were added to Quantifoil R1.2/1.3 400 mesh Au holey carbon grids (Quantifoil), blotted using a Vitrobot Mark IV (FEI), and frozen in liquid ethane. The grids were imaged in a 300 keV Titan Krios (FEI) with a Gatan K3 Summit direct electron detector (Gatan). Data were collected in super-resolution mode and the parameters of each set of data collection were summarized in the Supplementary Table 1.

Imaging Processing and 3D reconstruction

Dark subtracted movies of the hSMO–G_i complexes were normalized by gain reference and the motion correction was performed using MotionCor2 [41]. The contrast transfer function (CTF) was estimated using CTFFIND4 [42]. To generate the templates for automatic picking, around 2000 particles of each data set were manually picked and classified by 2D classification in RELION-3 [43]. After auto-picking in RELION-3, the low-quality images and false-positive particles were removed manually. The remaining particles were extracted for subsequent 2D and 3D classification.

A low-resolution cryo-EM map of hSMO–G_i–SAG complex generated from a data set collected on 200 keV Talos Arctica (FEI) was used as the initial model for 3D classification of the Titan Krios data set in RELION-3. The best class from 3D classification was selected for the initial 3D-refinement. Then, the motion correction was re-performed with the first 21 of the 30 frames (resulting in a total dose of ~60 electrons per $Å^2$) and the particles were re-extracted. Bayesian polishing was applied to the re-extracted particles, followed by the final 3D-refinement with a soft mask and solvent-flattened Fourier shell correlations (FSCs). For the hSMO–G_i–EC, hSMO^{D384R}–G_i and hSMO$^{G111C/I496C}$–G_i complexes, the cryo-EM map of the hSMO–G_i–SAG complex after 3D-refinment was used as the initial model for 3D classification. The best class from 3D classification was selected for the initial 3D-refinement, followed by Bayesian polishing and CTF refinement with beam tilt correction in RELION-3. The resulting particles were used for the final 3D-refinement with a soft mask and solvent-flattened FSCs. The resolution was estimated using “post-processing” with the FSC criteria of 0.143. The masks for post-processing were generated by RELION-3 using the 3D-refinement map as the input with the parameters listed below: for hSMO–G_i–SAG complex, Threshold = 0.005, Extend = 6 pixels, Soft-edge = 12 pixels; for hSMO–G_i–EC complex, Threshold = 0.00921, Extend = 10 pixels, Soft-edge = 15 pixels; for hSMO^{D384R}–G_i complex, Threshold = 0.00948, Extend = 5 pixels, Soft-edge = 15 pixels; for hSMO$^{G111C/I496C}$–G_i complex, Threshold = 0.014, Extend = 5 pixels, Soft-edge = 15 pixels. Local map resolution was estimated by RELION-3.

Model Construction, Refinement and Validation

The final maps were B-factor sharpened by “post-processing” in RELION-3 for the model building and refinement. The position of CRD in the cryo-EM map was observed by the relatively weak densities in the hSMO–G_i–SAG, hSMO^{D384R}–G_i, and hSMO$^{G111C/I496C}$–G_i complexes, but not in the hSMO–G_i–EC complex (Supplementary Figures. 1, 3, 5 and 7). The CRD structure of hSMO (PDB: 5L7D), 7-TMs structure of hSMO–G_i–Fab-G50 complex (PDB: 6OT0) and the structures of $G\alpha_i1\beta1\gamma2$ and svFc16 from μOR–G_i complex

(PDB: 6DDE) were docked into the map as the initial model for hSMO–G_i–SAG complex. The refined hSMO–G_i–SAG structure was used as the initial model for the $hSMO^{D384R}$–G_i, $hSMO^{G111C/I496C}$–G_i complex and hSMO–G_i–EC complexes. The CRD was not built in the hSMO–G_i–EC complex. All structure models were manually built by COOT [44], followed by refinement in real space using PHENIX [45] and in reciprocal space using Refmac with secondary-structure restraints and stereochemical restraints [46,47]. For cross-validations, the final model was refined against one of the half maps from the final 3D-refinement. The resulting model was used to calculate the model vs. map FSC curves against the same half map and the other half map, respectively, using the Comprehensive validation module in PHENIX [45]. MolProbity[48] was used to validate the geometries of the model. Structure figures were generated using PyMOL (http://www.pymol.org) and Chimera [49].

HH Reporter Assays

To detect the activity of SMO variants in HH signaling, the 8X-GLI-Firefly luciferase reporter transgene, a constitutive *Renilla* luciferase transgene and a pcDNA3.1 vector encoding different variants of hSMO were co-transfected to $Smo^{-/-}$ MEFs in 24-well plates using TransIT®−2020 Transfection Reagent (Mirus Bio LLC). After 24 hours, cells were serum-starved in Dulbecco's Modified Eagle's high glucose Medium (DMEM-hg) with 0.5% FBS. 24 hours later, cells were treated with 100 nM SAG (Selleck Chemicals) for another 24 hours. Firefly and *Renilla* luciferase activity were measured using the Dual-Luciferase® Reporter Assay System (Promega). The data analysis was performed using GraphPad Prism 7 (GraphPad Software). Results are shown as mean ± s.d. from 3 biologically independent experiments.

Sterol depletion assays

A pcDNA3.1 vector encoding different variants of hSMO were transfected to $Smo^{-/-}$ MEFs in 6-well plates as described above. After 24 hours, the cells were treated with DMEM-hg containing 5% lipoprotein-deficient serum (LPDS) [50], with or without 1% (w/v) hydroxypropyl-β-cyclodextrin (HPCD, Trappsol), 10 μM sodium compactin and 50 μM sodium mevalonate at 37 °C for 1 hour. Then, the cells were washed by PBS and further cultured in DMEM-hg containing 0.5% LPDS with or without 10 μM sodium compactin and 50 μM sodium mevalonate at 37 °C for an additional 24 hours.

The total RNA and cDNA were prepared as described before [51]. Mouse *GLI1* mRNA level was measured by reverse-transcription PCR (qRT–PCR) using mouse *GAPDH* as an internal control. The primers used for qRT-PCR are *GLI1*: forward 5' CAATTTCAACCCCTCCTCCTCT; reverse 5' AGGTGCAAAGCCAGATCCATA and *GAPDH*: forward 5' CATTTGCAGTGGCAAAGTGGAG; reverse 5' ACCCCATTTGATGTTAGTGGGG. The qRT–PCR was performed using a QuantStudio 5 Real-Time PCR System (Thermo Fisher Scientific) or a ViiA™ 7 Real-Time PCR System (Applied Biosystems) with SYBR Green (Bio-Rad). Relative *GLI1* transcript levels in each experimental group compared to wild-type control group were calculated using the ΔΔCt method. Results are shown as mean ± s.d. from three technical repeats. Similar results were obtained in three biologically independent experiments.

Immunoblot analysis

A pcDNA3.1 vector encoding different variants of hSMO were transfected to *Smo*$^{-/-}$ MEFs using jetPRIME Reagent (Polyplus). After 24 hours, the medium was changed to DMEM with 0.5% FCS. The cells were resuspended in RIPA buffer with 1 mM PMSF after another 24 hours. After high-speed centrifugation, the resulting supernatant was incubated with a solubilization buffer containing 62 mM Tris-HCl pH 6.9, 15% SDS, 8M urea, 10% glycerol and 100mM dithiothreitol at 1:1 volume ratio at 37 °C for 30 minutes. After electrophoresis, the proteins were transferred to nitrocellulose filters, which were then incubated with SMO antibody E-5 (1:300, Santa Cruz Biotechnology, sc-166685) at 4 °C overnight, followed by the incubation of HRP-linked anti-mouse IgG (1:5000, Cell Signaling Technology) at room temperature for 1 hour. Calnexin was used as the internal control and detected by anti-calnexin (Novus #NB100–1965). Bound antibodies were visualized by a SuperSignal™ West Pico PLUS Chemiluminescent Substrate kit (Thermo Fisher Scientific). The images were scanned and analyzed using an Odyssey Fc Imaging System (LI-COR Biosciences). Similar results were obtained in three biologically independent experiments.

Extended Data

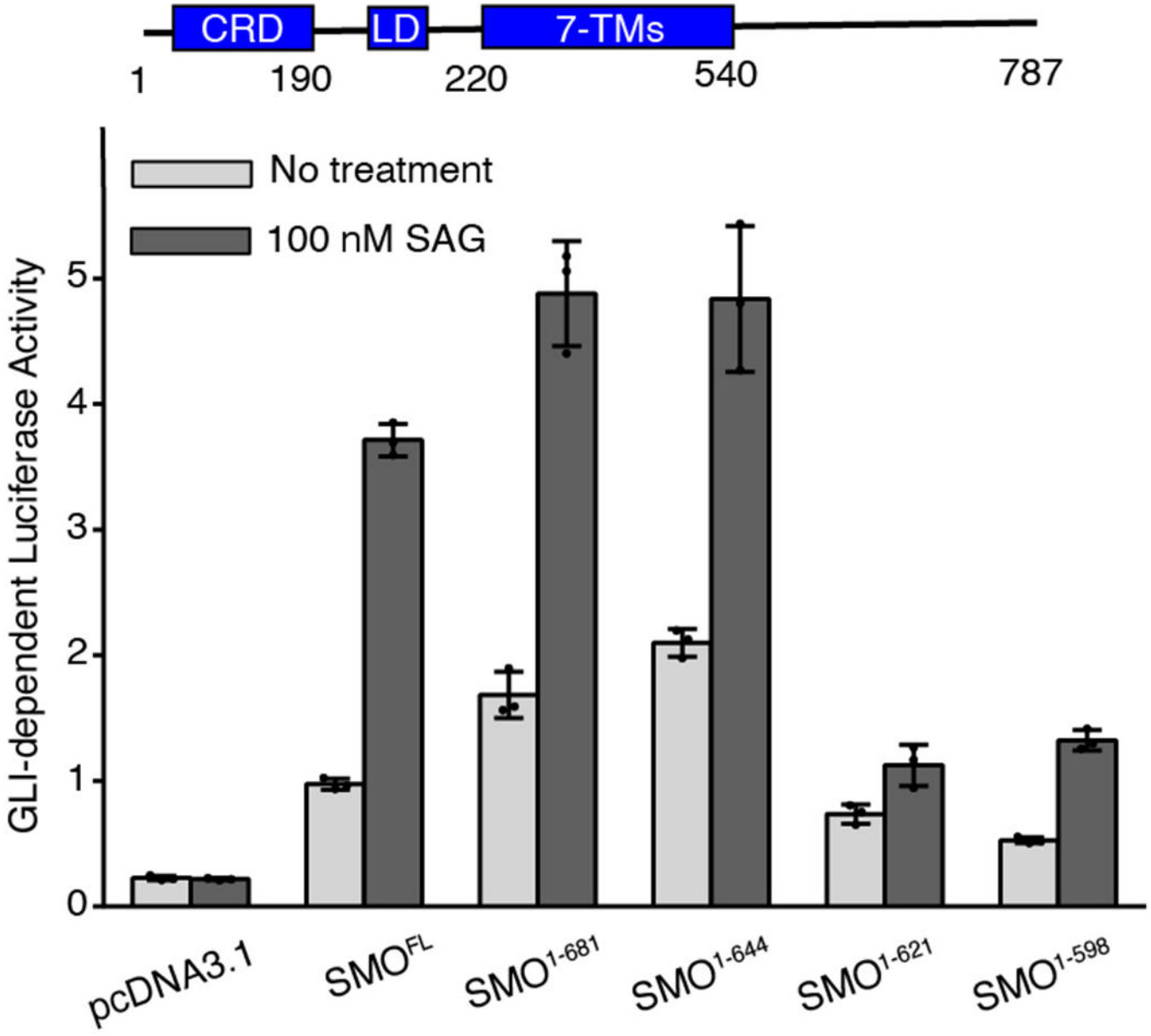

Extended Data Fig. 1. Functional characterization of the C-terminal tail of SMO in HH signaling.

The domain structure of SMO is shown above. HH signaling in $SMO^{-/-}$ mouse embryonic fibroblasts (MEFs) transfected with pcDNA3.1 and SMO variants was measured via luciferase activity. Data are mean ± s.d. (n = 3 biologically independent experiments).

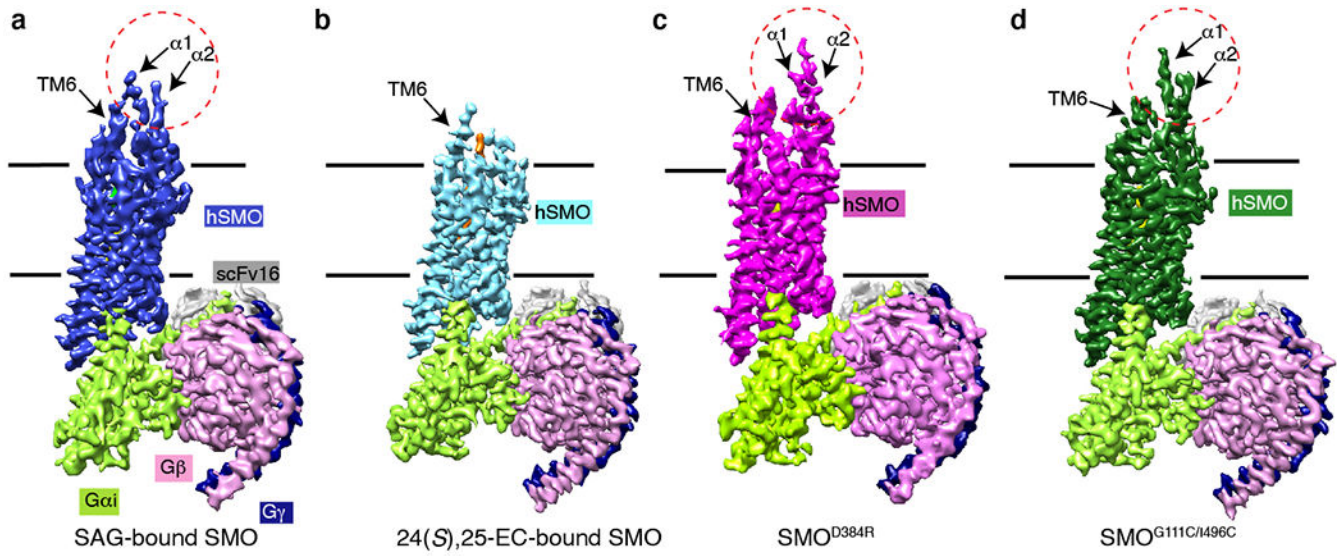

Extended Data Fig. 2. The overall cryo-EM maps of SMO–G_i complexes.

a, The map of SMO–G_i–SAG complex. **b,** The map of SMO–G_i–24(*S*),25-EC complex. **c,** The map of SMO^{D384R}–G_i complex. **d,** The map of $SMO^{G111C/I496C}$–G_i complex. Each subunit is displayed in different colors. The α1 and α2 of CRD are labeled and the position of CRD is indicated by red circles.

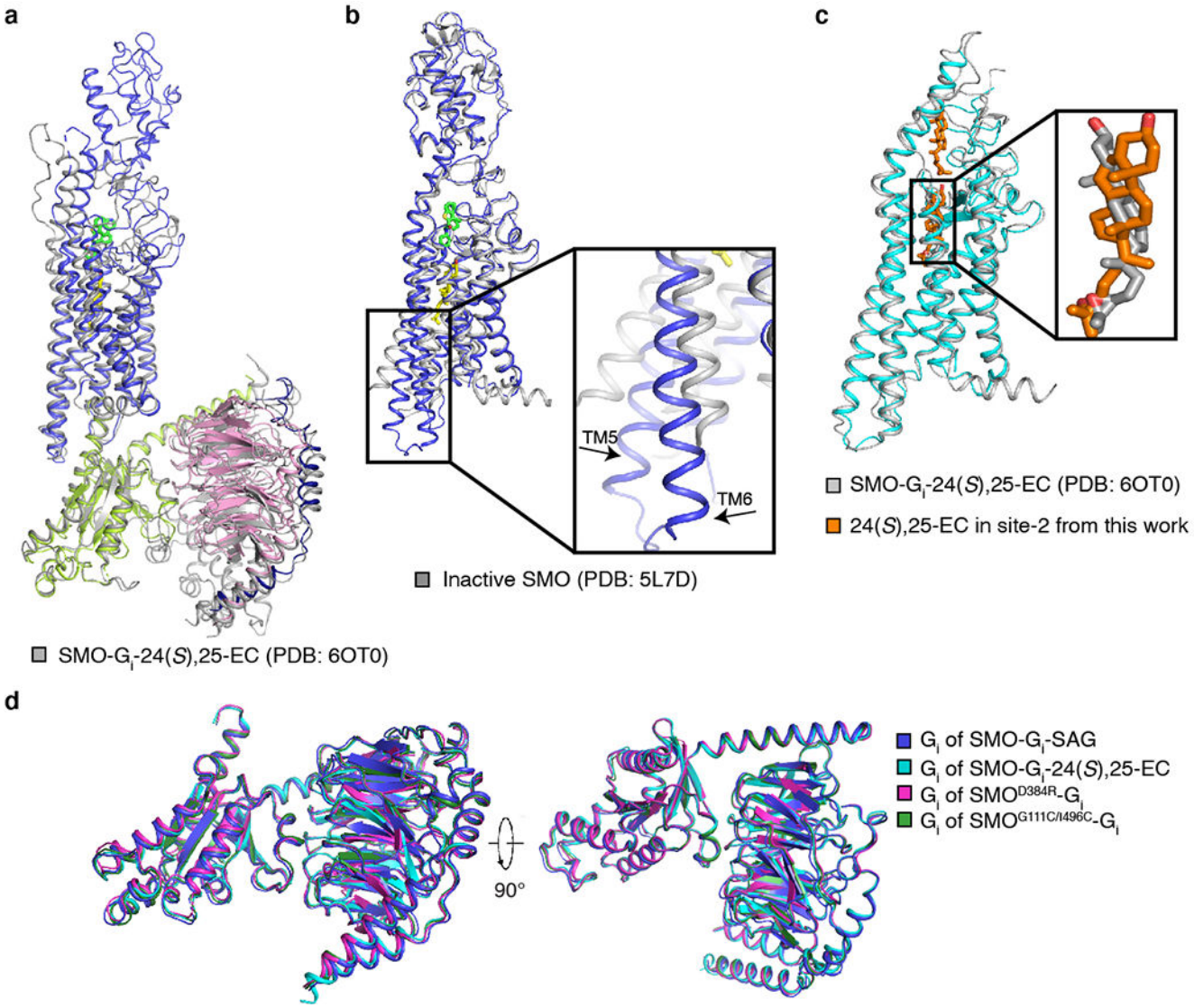

Extended Data Fig. 3. Structural comparison of SMO and G_i protein in the different states.

a, Structural comparison of SMO–G_i–SAG complex with the previously reported structure of SMO–G_i–24(*S*),25-EC complex (pdb: 6OT0). **b,** structural comparison of SMO in SMO–G_i– SAG complex with inactive SMO (pdb: 5L7D). **c,** Structural comparison of 3.1-Å SMO–G_i–24(*S*),25-EC complex with the previously reported structure of SMO–G_i–24(*S*),25-EC complex (pdb: 6OT0). **d,** Structural comparison of G_i proteins in these reported four complexes.

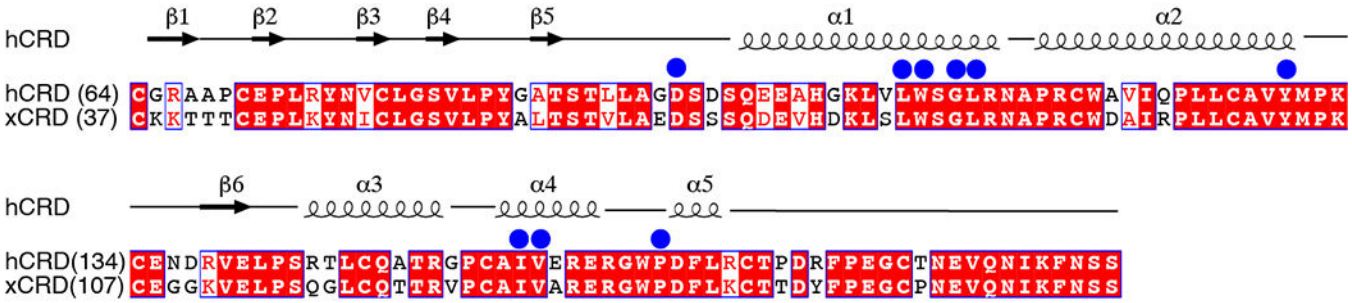

Extended Data Fig. 4. Sequence alignment of hSMO-CRD with xSMO-CRD.

The cholesterol binding residues are indicated by blue circles in both of hCRD and xCRD. The secondary structures of both CRDs are indicated above the sequences.

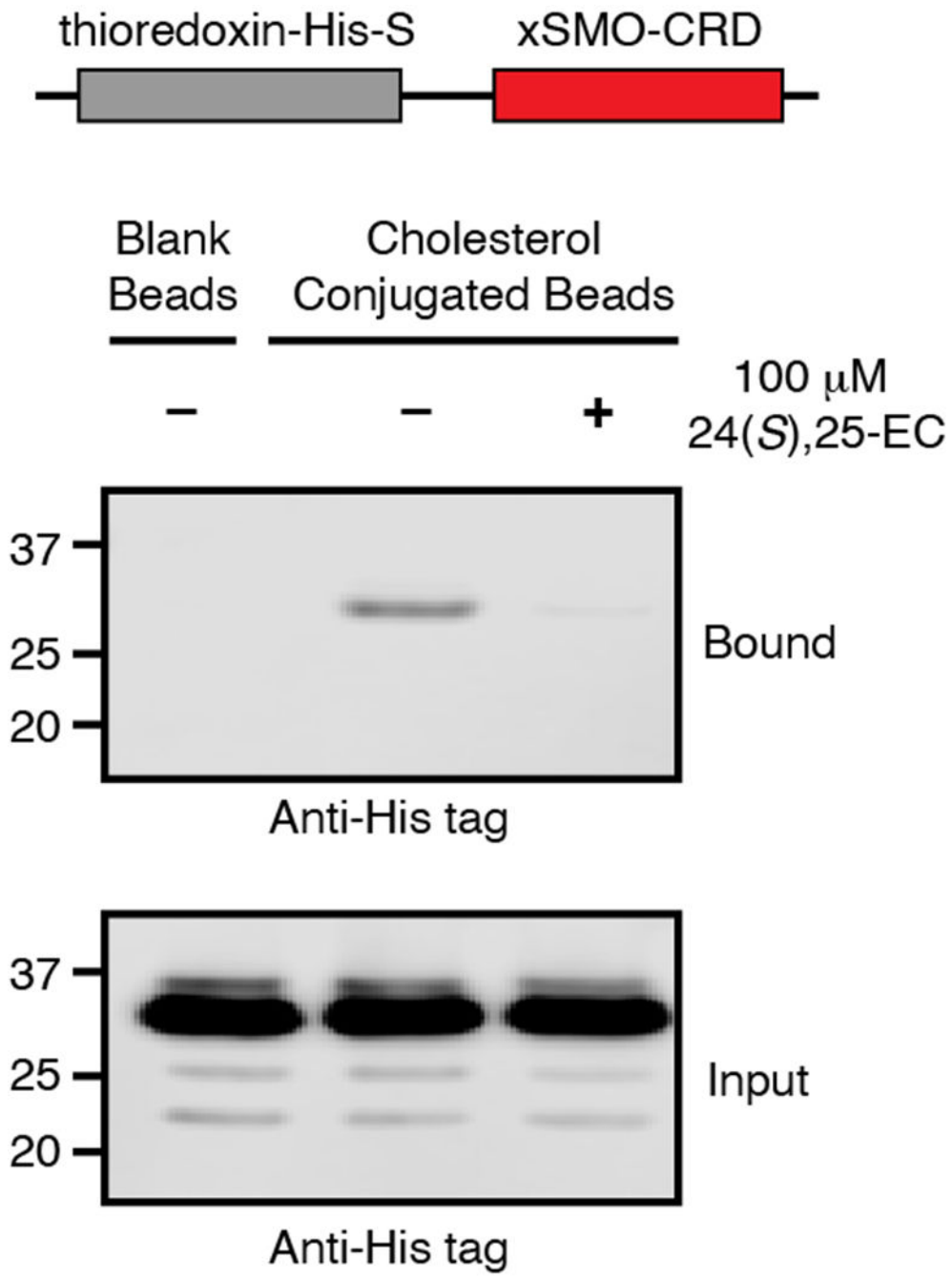

Extended Data Fig. 5. 24(*S*),25-EC binding assay.

The construct of the xCRD domain structure is shown. The protein was detected by Western blotting. The assay was reproduced three times with similar results.

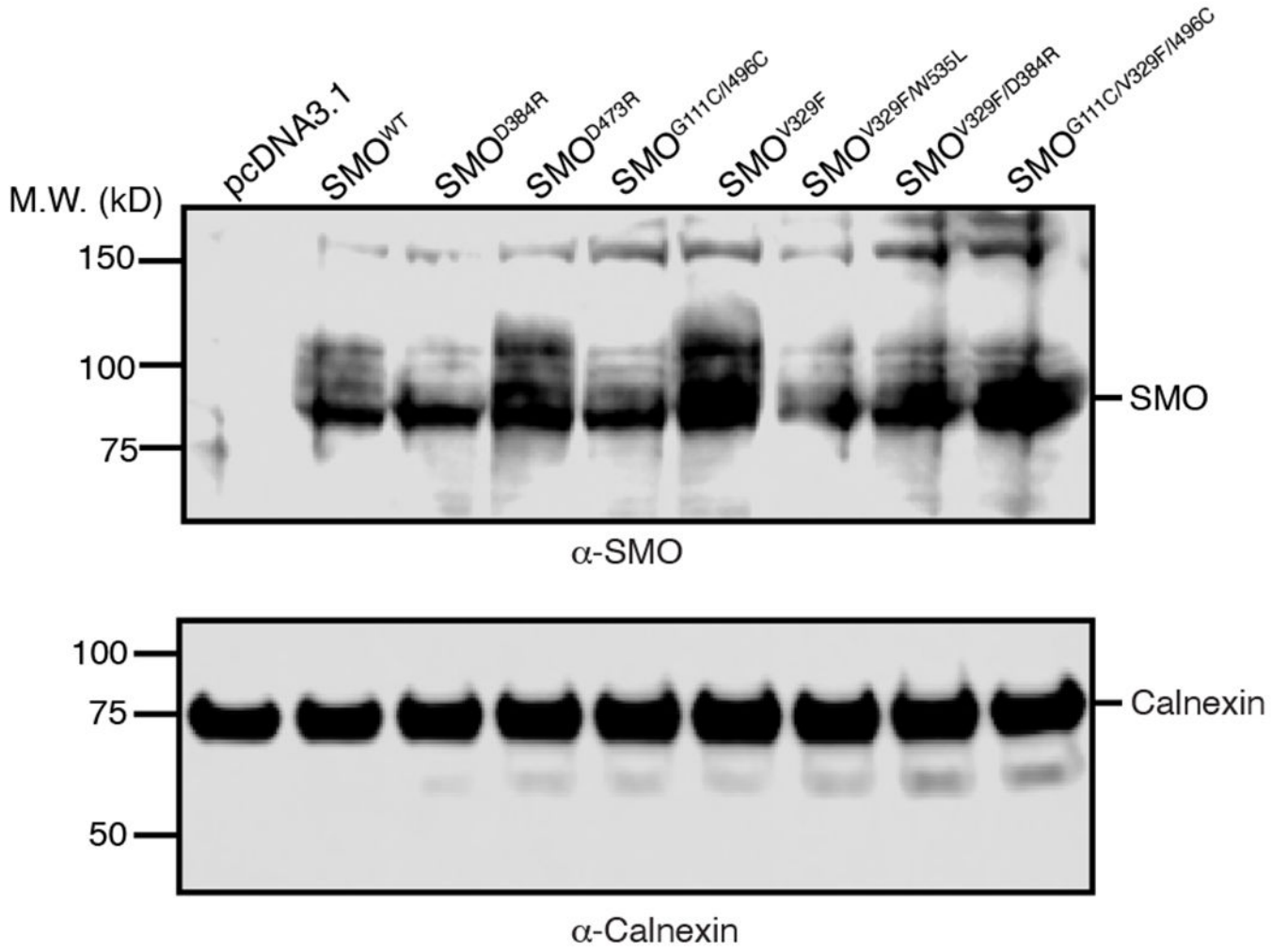

Extended Data Fig. 6. Expression levels of SMO and its variants in this study.

The transiently expressed SMO proteins were detected by western blotting. Calnexin served as an internal control and was detected via anti-calnexin antibody. Similar results were obtained in three biologically independent experiments.

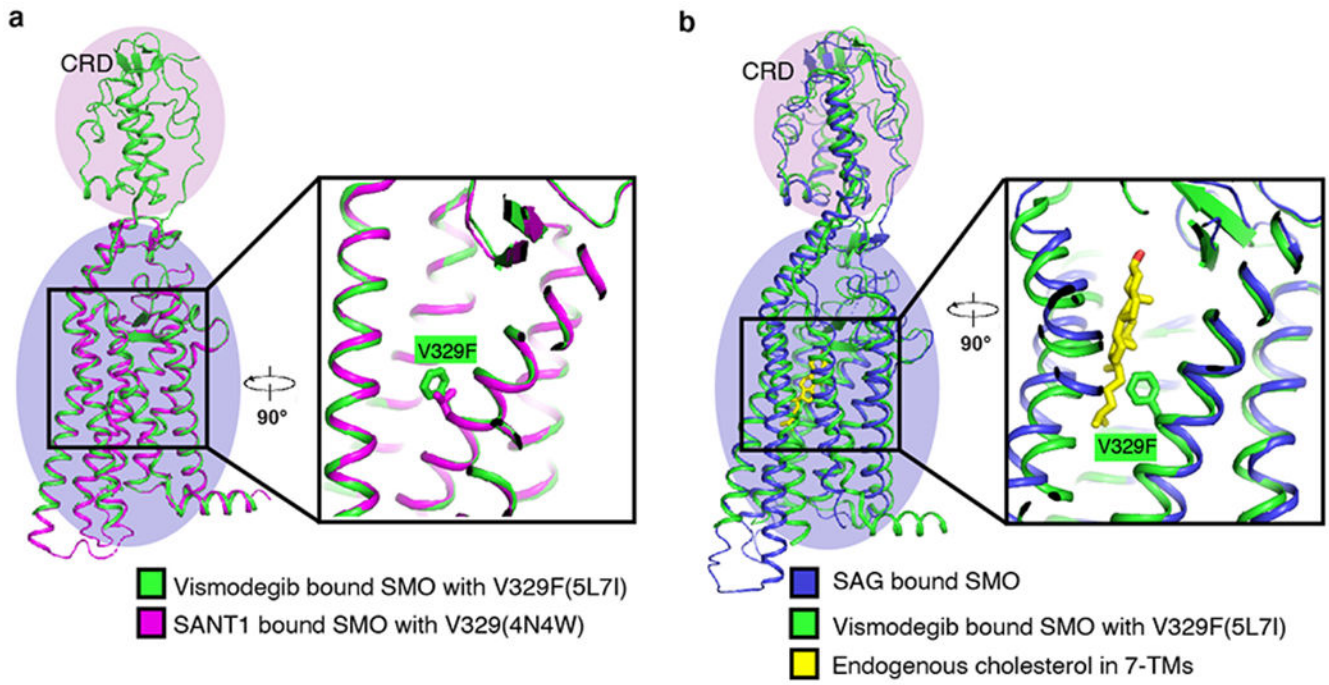

Extended Data Fig. 7. Structural comparison of SMO^{V329F} with wild type SMO.

a, Structural comparison of Vismodegib-bound SMO^{V329F} with SANT1-bound SMO. The similar conformations of both structures indicate that V329F could not abolish the folding of SMO. **b,** Structural comparison reveals that V329F could abolish the endogenous cholesterol binding in site 1. The ligand is shown as sticks. The CRD and 7-TMs of SMO have been indicated by circles.

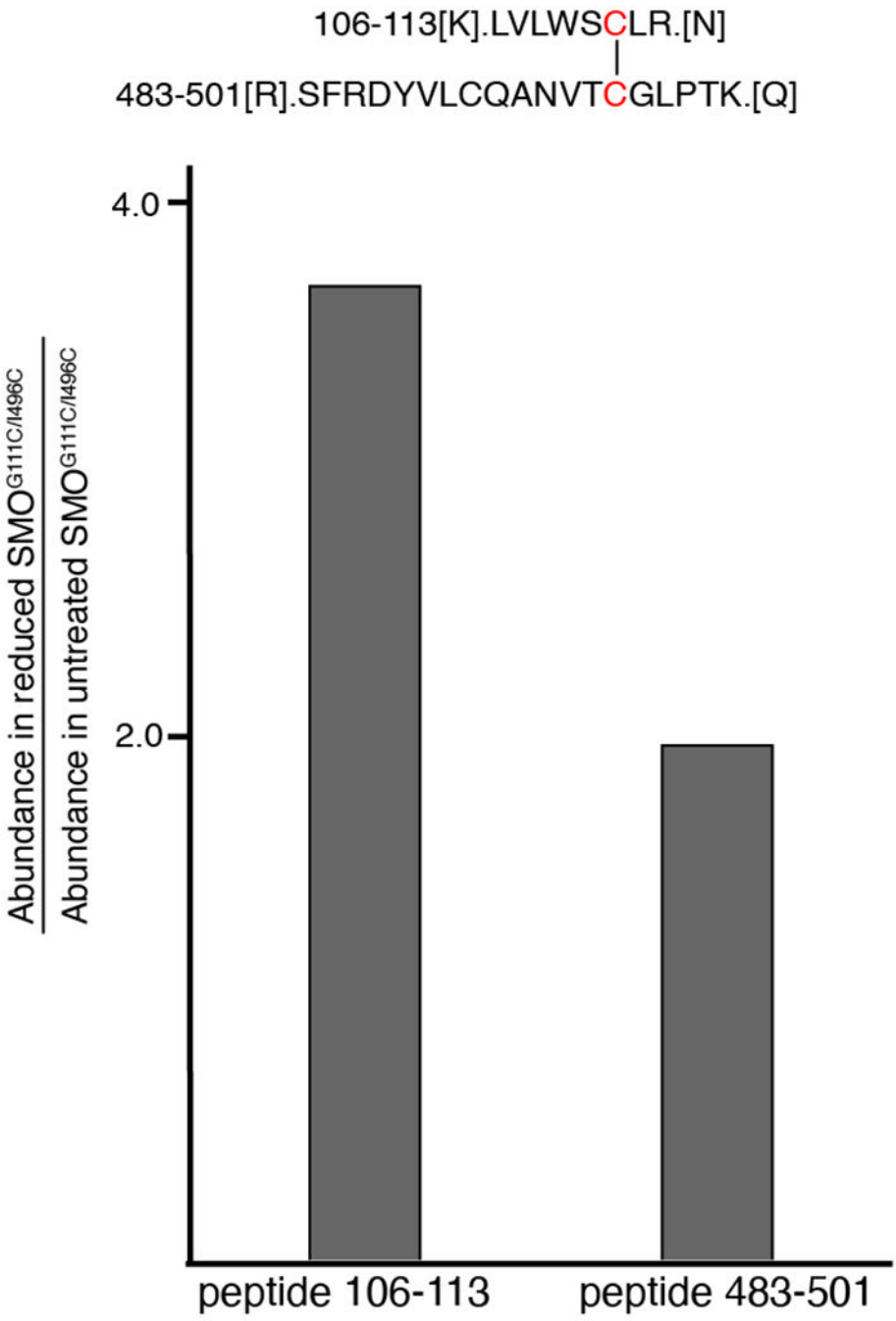

Extended Data Fig. 8. Identification of the designed disulfide bond in SMO$^{G111C/I496C}$ by mass spectrometry.

SMO$^{G111C/I496C}$ and SMO^{WT} proteins were treated with or without 5mM TCEP at room temperature for 40 minutes, followed by the incubation of 150 mM iodoacetamide for an additional 40 minutes. The corresponding bands of SMO were cropped from the SDS-PAGE gel and sent for mass spectrometry analysis. Annotated Sequences of SMO were detected by Liquid Chromatography-Mass Spectrometry (LC-MS). After normalizing the amount of the samples, the results show that the abundance of peptide 106–113 and peptide 483–501, containing either Cys111 or Cys496, after TCEP treatment increase 2.0~3.7 fold than

without treatment, suggesting that the majority of $SMO^{G111C/I496C}$ contains the designed disulfide bond between Cys111 and Cys496. Both peptides could not be found in the TCEP-treated SMO^{WT} sample. The experiment was re-produced twice in different weeks with similar results.

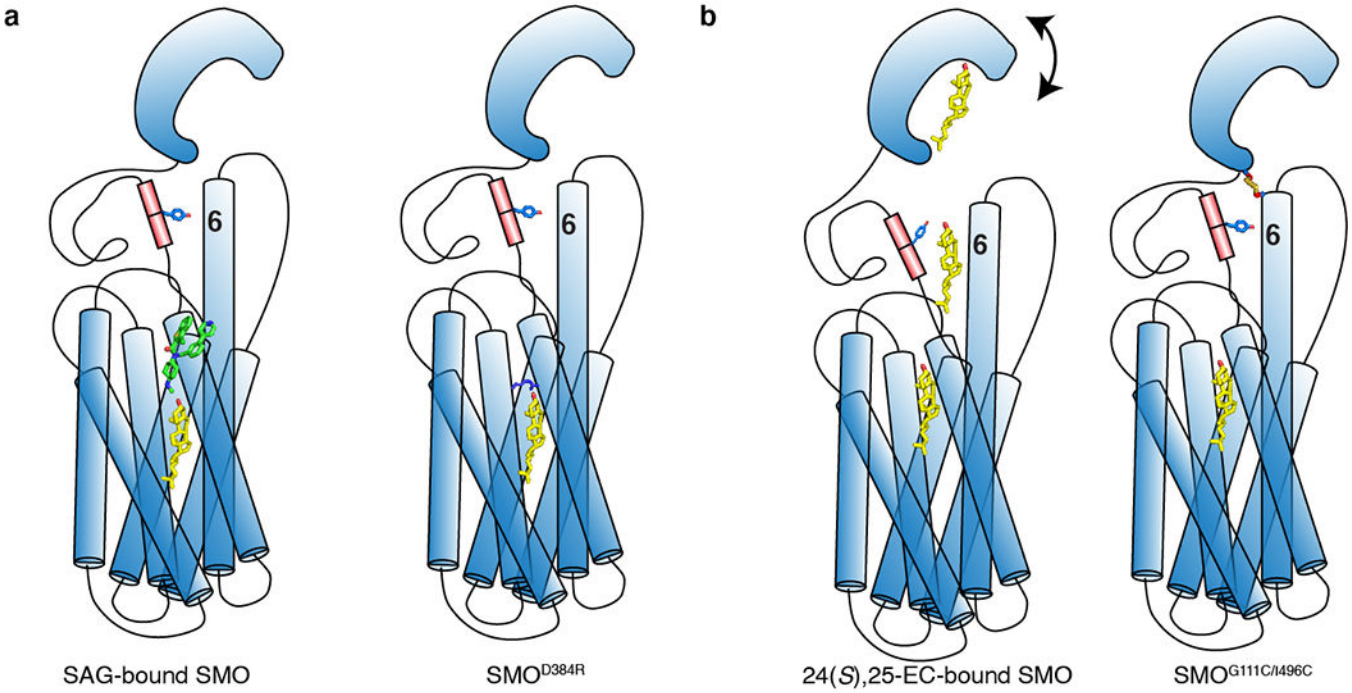

Extended Data Fig. 9. Cartoon model of the SMO–G_i complexes in this work.
Sterols have been blocked in site-1 in panel **a**; while sterols have been observed in site-2 and site-3 in panel **b**.

Supplementary Material

Refer to Web version on PubMed Central for supplementary material.

Acknowledgements

We thank D. Stoddard at the UT Southwestern Medical Center Cryo-EM Facility (funded in part by the CPRIT Core Facility Support Award RP170644) for assistance in data collection. We thank B. Kobilka for sharing the plasmids of G_i and scFv16; L. Beatty, L. Esparza and C. Lee for tissue culture; A. Lemoff at the UT Southwestern Proteomics Core for mass spectrometry identification and M. Brown, B. Chen, E. Debler, J. Goldstein, J. Jiang, Y. Yu, C. Zhang for discussion. This work was supported by the Endowed Scholars Program in Medical Science of UT Southwestern Medical Center, NIH grant P01 HL020948, NIH grant R01 GM135343 and Welch Foundation (I-1957) (to X.L.). X.Q. is the recipient of a DDBrown Fellow of the Life Sciences Research Foundation. X.L. is a Damon Runyon-Rachleff Innovator supported by the Damon Runyon Cancer Research Foundation (DRR-53–19) and a Rita C. and William P. Clements, Jr. Scholar in Biomedical Research at UT Southwestern Medical Center.

References:

1. Arensdorf AM, Marada S & Ogden SK Smoothened Regulation: A Tale of Two Signals. Trends in pharmacological sciences 37, 62–72, doi:10.1016/j.tips.2015.09.001 (2016). [PubMed: 26432668]

2. Hu A & Song BL The interplay of Patched, Smoothened and cholesterol in Hedgehog signaling. Current opinion in cell biology 61, 31–38, doi:10.1016/j.ceb.2019.06.008 (2019). [PubMed: 31369952]

3. Kozielewicz P, Turku A & Schulte G Molecular Pharmacology of Class F Receptor Activation. Molecular pharmacology 97, 62–71 doi:10.1124/mol.119.117986 (2020). [PubMed: 31591260]

4. Qi X & Li X Mechanistic Insights into the Generation and Transduction of Hedgehog Signaling. Trends in biochemical sciences 45, 397–410, doi:10.1016/j.tibs.2020.01.006 (2020). [PubMed: 32311334]

5. Qi X, Schmiege P, Coutavas E, Wang J & Li X Structures of human Patched and its complex with native palmitoylated sonic hedgehog. Nature 560, 128–132, doi:10.1038/s41586-018-0308-7 (2018). [PubMed: 29995851]

6. Qi X, Schmiege P, Coutavas E & Li X Two Patched molecules engage distinct sites on Hedgehog yielding a signaling-competent complex. Science 362, 52 doi:10.1126/science.aas8843 (2018).

7. Zhang Y et al. Structural Basis for Cholesterol Transport-like Activity of the Hedgehog Receptor Patched. Cell 175, 1352–1364 e1314, doi:10.1016/j.cell.2018.10.026 (2018). [PubMed: 30415841]

8. Qian H et al. Inhibition of tetrameric Patched1 by Sonic Hedgehog through an asymmetric paradigm. Nature communications 10, 2320, doi:10.1038/s41467-019-10234-9 (2019).

9. Rudolf AF et al. The morphogen Sonic hedgehog inhibits its receptor Patched by a pincer grasp mechanism. Nature chemical biology 15, 975–982, doi:10.1038/s41589-019-0370-y (2019). [PubMed: 31548691]

10. Tukachinsky H, Petrov K, Watanabe M & Salic A Mechanism of inhibition of the tumor suppressor Patched by Sonic Hedgehog. Proceedings of the National Academy of Sciences of the United States of America 113, E5866–E5875, doi:10.1073/pnas.1606719113 (2016). [PubMed: 27647915]

11. Pak E & Segal RA Hedgehog Signal Transduction: Key Players, Oncogenic Drivers, and Cancer Therapy. Developmental cell 38, 333–344, doi:10.1016/j.devcel.2016.07.026 (2016). [PubMed: 27554855]

12. Nachtergaele S et al. Structure and function of the Smoothened extracellular domain in vertebrate Hedgehog signaling. eLife 2, e01340, doi:10.7554/eLife.01340 (2013). [PubMed: 24171105]

13. Huang P et al. Cellular Cholesterol Directly Activates Smoothened in Hedgehog Signaling. Cell 166, 1176–1187 e1114, doi:10.1016/j.cell.2016.08.003 (2016). [PubMed: 27545348]

14. Qi X et al. Cryo-EM structure of oxysterol-bound human Smoothened coupled to a heterotrimeric Gi. Nature 571, 279–283, doi:10.1038/s41586-019-1286-0 (2019). [PubMed: 31168089]

15. Deshpande I et al. Smoothened stimulation by membrane sterols drives Hedgehog pathway activity. Nature 571, 284–288, doi:10.1038/s41586-019-1355-4 (2019). [PubMed: 31263273]

16. Sharpe HJ, Wang W, Hannoush RN & de Sauvage FJ Regulation of the oncoprotein Smoothened by small molecules. Nature chemical biology 11, 246–255, doi:10.1038/nchembio.1776 (2015). [PubMed: 25785427]

17. Huang P et al. Structural Basis of Smoothened Activation in Hedgehog Signaling. Cell 175, 295–297, doi:10.1016/j.cell.2018.09.003 (2018). [PubMed: 30241610]

18. Luchetti G et al. Cholesterol activates the G-protein coupled receptor Smoothened to promote Hedgehog signaling. eLife 5, doi:10.7554/eLife.20304 (2016).

19. Byrne EFX et al. Structural basis of Smoothened regulation by its extracellular domains. Nature 535, 517–522, doi:10.1038/nature18934 (2016). [PubMed: 27437577]

20. Rana R et al. Structural insights into the role of the Smoothened cysteine-rich domain in Hedgehog signalling. Nature communications 4, 2965, doi:10.1038/ncomms3965 (2013).

21. Xiao X et al. Cholesterol Modification of Smoothened Is Required for Hedgehog Signaling. Molecular cell 66, 154–162 e110, doi:10.1016/j.molcel.2017.02.015 (2017). [PubMed: 28344083]

22. Myers BR et al. Hedgehog pathway modulation by multiple lipid binding sites on the smoothened effector of signal response. Developmental cell 26, 346–357, doi:10.1016/j.devcel.2013.07.015 (2013). [PubMed: 23954590]

23. Wang C et al. Structure of the human smoothened receptor bound to an antitumour agent. Nature 497, 338–343, doi:10.1038/nature12167 (2013). [PubMed: 23636324]

24. Li S, Ma G, Wang B & Jiang J Hedgehog induces formation of PKA-Smoothened complexes to promote Smoothened phosphorylation and pathway activation. Science signaling 7, ra62, doi:10.1126/scisignal.2005414 (2014). [PubMed: 24985345]
25. Kim J et al. The role of ciliary trafficking in Hedgehog receptor signaling. Science signaling 8, ra55, doi:10.1126/scisignal.aaa5622 (2015). [PubMed: 26038600]
26. Riobo NA, Saucy B, Dilizio C & Manning DR Activation of heterotrimeric G proteins by Smoothened. Proceedings of the National Academy of Sciences of the United States of America 103, 12607–12612, doi:10.1073/pnas.0600880103 (2006). [PubMed: 16885213]
27. Marada S et al. Functional Divergence in the Role of N-Linked Glycosylation in Smoothened Signaling. PLoS Genet 11, e1005473, doi:10.1371/journal.pgen.1005473 (2015). [PubMed: 26291458]
28. Pandit T & Ogden SK Contributions of Noncanonical Smoothened Signaling During Embryonic Development. Journal of developmental biology 5, 11 doi:10.3390/jdb5040011 (2017). [PubMed: 29399514]
29. Koehl A et al. Structure of the micro-opioid receptor-Gi protein complex. Nature 558, 547–552, doi:10.1038/s41586-018-0219-7 (2018). [PubMed: 29899455]
30. Chen Y et al. Sonic Hedgehog dependent phosphorylation by CK1alpha and GRK2 is required for ciliary accumulation and activation of smoothened. PLoS biology 9, e1001083, doi:10.1371/journal.pbio.1001083 (2011). [PubMed: 21695114]
31. Yang H et al. Converse conformational control of smoothened activity by structurally related small molecules. The Journal of biological chemistry 284, 20876–20884, doi:10.1074/jbc.M807648200 (2009). [PubMed: 19366682]
32. Raleigh DR et al. Cilia-Associated Oxysterols Activate Smoothened. Molecular cell 72, 316–327 e315, doi:10.1016/j.molcel.2018.08.034 (2018). [PubMed: 30340023]
33. Kowatsch C, Woolley RE, Kinnebrew M, Rohatgi R & Siebold C Structures of vertebrate Patched and Smoothened reveal intimate links between cholesterol and Hedgehog signalling. Current opinion in structural biology 57, 204–214, doi:10.1016/j.sbi.2019.05.015 (2019). [PubMed: 31247512]
34. Dijkgraaf GJ et al. Small molecule inhibition of GDC-0449 refractory smoothened mutants and downstream mechanisms of drug resistance. Cancer research 71, 435–444, doi:10.1158/0008-5472.CAN-10-2876 (2011). [PubMed: 21123452]
35. Qi C, Di Minin G, Vercellino I, Wutz A & Korkhov VM Structural basis of sterol recognition by human hedgehog receptor PTCH1. Science advances 5, eaaw6490, doi:10.1126/sciadv.aaw6490 (2019). [PubMed: 31555730]
36. Gong X et al. Structural basis for the recognition of Sonic Hedgehog by human Patched1. Science 361, 568 doi:10.1126/science.aas8935 (2018).
37. Winkler MBL et al. Structural Insight into Eukaryotic Sterol Transport through Niemann-Pick Type C Proteins. Cell 179, 485–497 e418, doi:10.1016/j.cell.2019.08.038 (2019). [PubMed: 31543266]
38. Long T et al. Structural basis for itraconazole-mediated NPC1 inhibition. Nature communications 11, 152, doi:10.1038/s41467-019-13917-5 (2020).
39. Zhang Y e. a. Hedgehog pathway activation through conformational blockade of the Patched sterol conduit. bioRxiv 10.1101/783290 (2019).
40. Kinnebrew M et al. Cholesterol accessibility at the ciliary membrane controls Hedgehog signaling. eLife 8, doi:10.7554/eLife.50051 (2019).
41. Zheng SQ et al. MotionCor2: anisotropic correction of beam-induced motion for improved cryo-electron microscopy. Nature methods 14, 331–332, doi:10.1038/nmeth.4193 (2017). [PubMed: 28250466]
42. Rohou A & Grigorieff N CTFFIND4: Fast and accurate defocus estimation from electron micrographs. Journal of structural biology 192, 216–221, doi:10.1016/j.jsb.2015.08.008 (2015). [PubMed: 26278980]
43. Zivanov J et al. New tools for automated high-resolution cryo-EM structure determination in RELION-3. eLife 7, doi:10.7554/eLife.42166 (2018).

44. Emsley P & Cowtan K Coot: model-building tools for molecular graphics. Acta crystallographica. Section D, Biological crystallography 60, 2126–2132, doi:10.1107/S0907444904019158 (2004). [PubMed: 15572765]
45. Adams PD et al. PHENIX: a comprehensive Python-based system for macromolecular structure solution. Acta crystallographica. Section D, Biological crystallography 66, 213–221, doi:10.1107/S0907444909052925 (2010). [PubMed: 20124702]
46. Murshudov GN, Vagin AA & Dodson EJ Refinement of macromolecular structures by the maximum-likelihood method. Acta crystallographica. Section D, Biological crystallography 53, 240–255, doi:10.1107/S0907444996012255 (1997). [PubMed: 15299926]
47. Brown A et al. Tools for macromolecular model building and refinement into electron cryo-microscopy reconstructions. Acta crystallographica. Section D, Biological crystallography 71, 136–153, doi:10.1107/S1399004714021683 (2015). [PubMed: 25615868]
48. Chen VB et al. MolProbity: all-atom structure validation for macromolecular crystallography. Acta crystallographica. Section D, Biological crystallography 66, 12–21, doi:10.1107/S0907444909042073 (2010). [PubMed: 20057044]
49. Pettersen EF et al. UCSF Chimera--a visualization system for exploratory research and analysis. Journal of computational chemistry 25, 1605–1612, doi:10.1002/jcc.20084 (2004). [PubMed: 15264254]
50. Metherall JE, Goldstein JL, Luskey KL & Brown MS Loss of transcriptional repression of three sterol-regulated genes in mutant hamster cells. The Journal of biological chemistry 264, 15634–15641 (1989). [PubMed: 2570073]
51. Chen B et al. Posaconazole, a Second-Generation Triazole Antifungal Drug, Inhibits the Hedgehog Signaling Pathway and Progression of Basal Cell Carcinoma. Molecular cancer therapeutics 15, 866–876, doi:10.1158/1535-7163.MCT-15-0729-T (2016). [PubMed: 26823493]

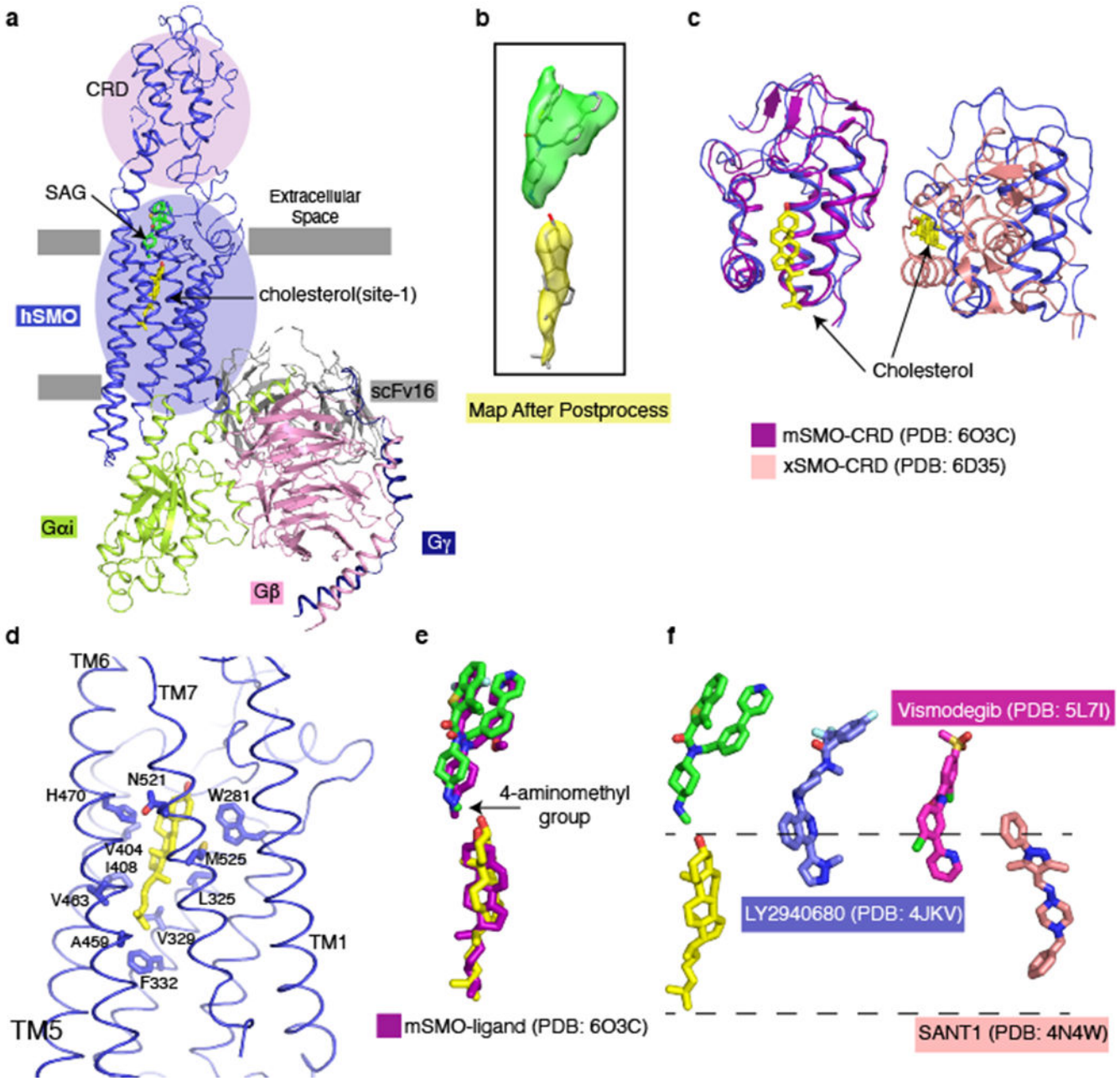

Fig. 1. Structure of SMO–G_i–SAG complex reveals an endogenous sterol in 7-TMs.

a, Ribbon representation of the complex. The CRD and 7-TMs of SMO have been indicated by circles. **b,** The cryo-EM map of ligands. The ligands are shown as sticks and their maps are shown at a 0.008 threshold level. **c,** Structural comparison of the CRD in the complex with that in active mSMO and xSMO. **d,** The interaction details between cholesterol and residues in the 7-TMs. **e,** Comparison of SAG and cholesterol binding sites in this complex with an active mSMO complex. **f,** Site 1 and synthetic ligand binding sites in SMO structures. The ligands are shown as sticks in different colors.

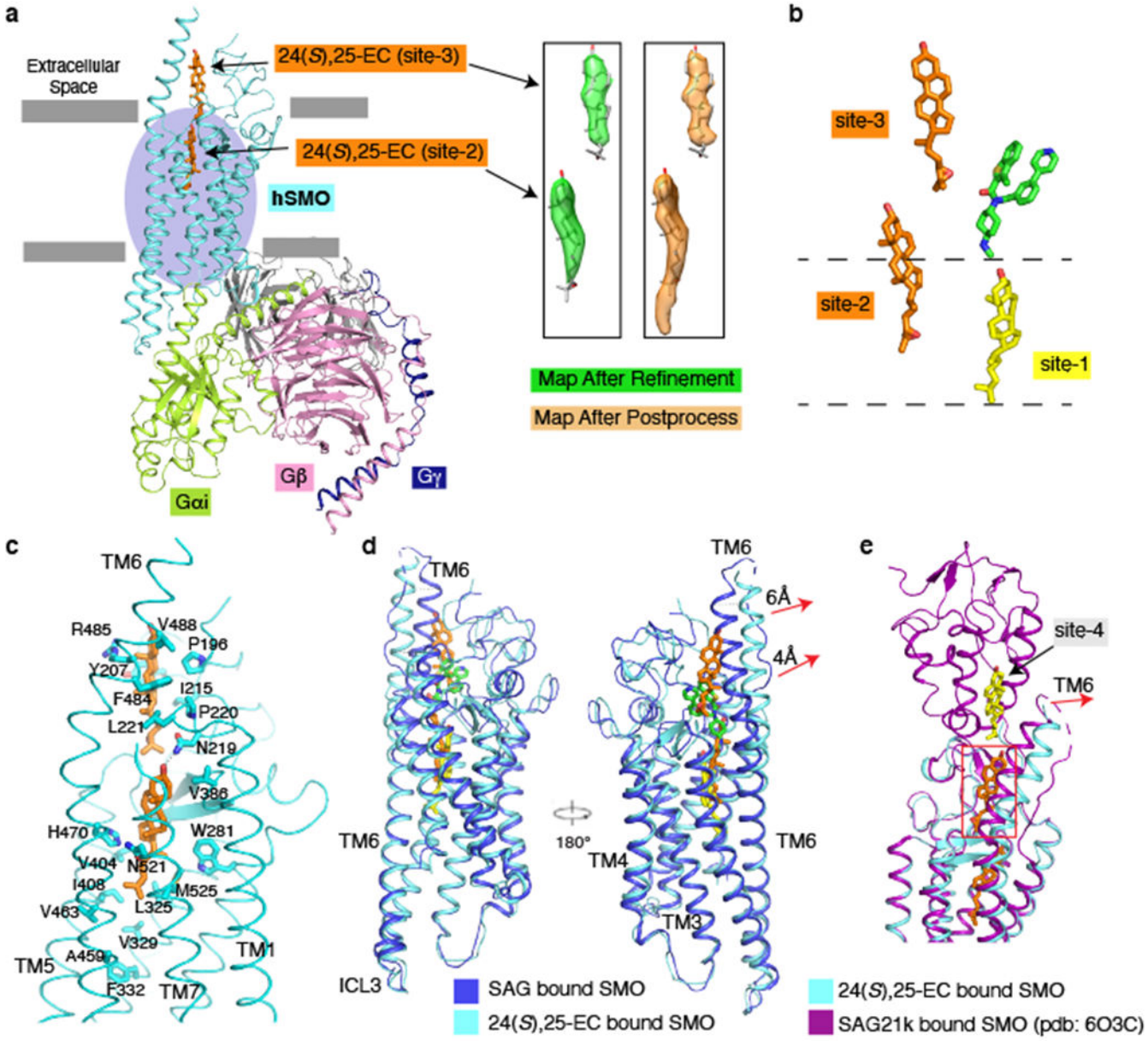

Fig. 2. Structure of SMO–G_i–24(*S*),25-EC reveals a novel sterol binding site.

a, Ribbon representation of the complex structure and cryo-EM map of the ligands. The 7-TMs of SMO have been indicated by a circle. The ligands are shown in sticks and their maps are shown at 0.00922 (refine) and 0.0109 (postprocessing) threshold levels. **b,** The relative position of sterol-binding site-1, site-2, and site-3 in the 7-TMs. **c,** The interaction details between sterols and residues in the 7-TMs and the LD. **d,** The structural comparison between 24(*S*),25-EC bound SMO and SAG-bound SMO. **e,** 24(*S*),25-EC bound to site-3 causes a conformational change of TM6 allowing the sterol to access site-4 of CRD from site-3. 24(*S*),25-EC is shown as orange sticks.

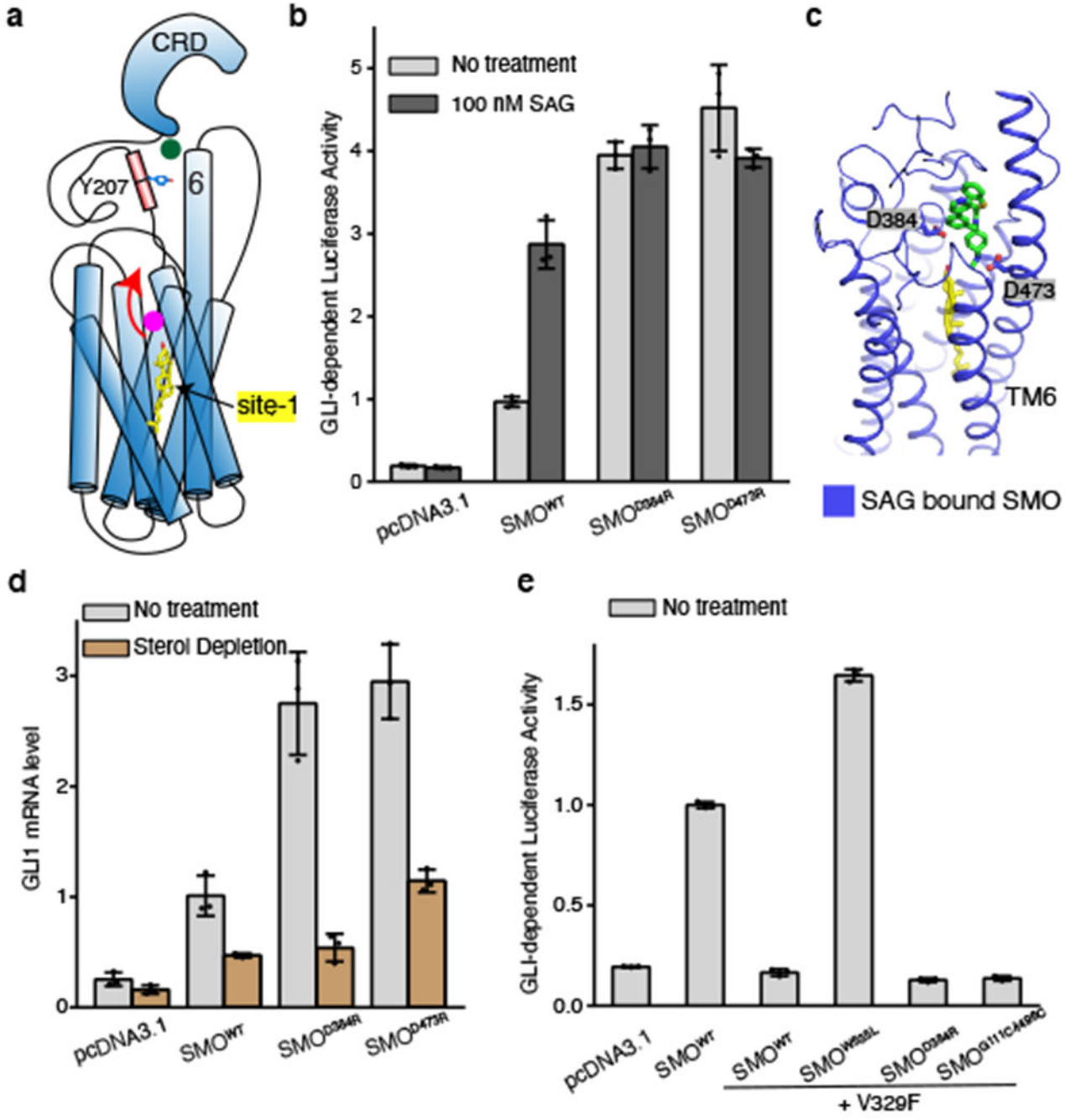

Fig. 3. The SMO^{D384R} is a gain-of-function SMO variant.

a, The logic for designing the constitutively active SMO mutants. The mutation sites are indicated by the circles. **b,** HH signaling in SMO$^{-/-}$ MEFs transfected with pcDNA3.1 and SMO variants. The GLI-dependent luciferase activity was measured. **c,** The location of residue D473 in SAG-bound SMO. **d,** Levels of GLI1 mRNA were used as a metric for HH signaling activity of SMO variants after sterol depletion. **e,** HH signaling in SMO$^{-/-}$ MEFs transfected with pcDNA3.1 and SMO variants with V329F. The GLI-dependent luciferase

activity is measured. In panels **b, d** and **e,** data are mean ± s.d. (n = 3 biologically independent experiments in **b** and **e**; n = 3 technical repeats in **d**).

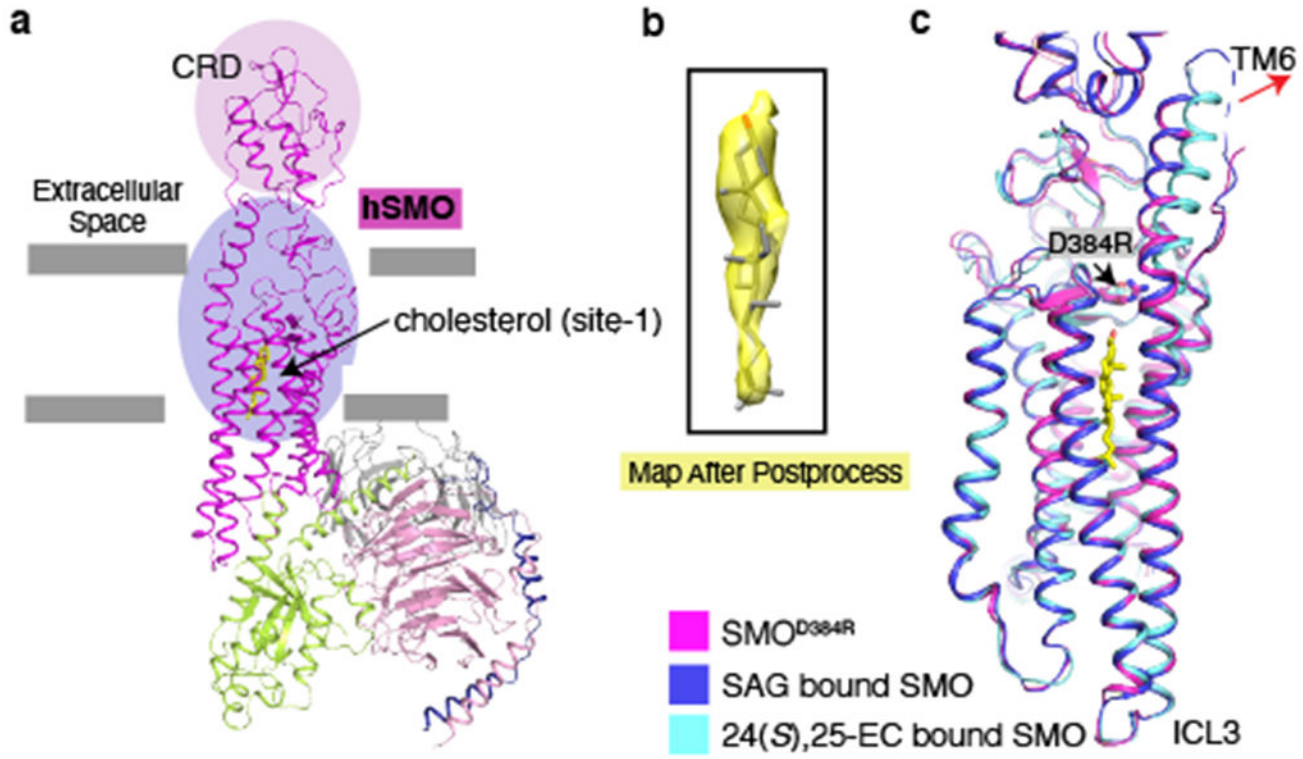

Fig. 4. Structure of SMO^{D384R}–Gi complex reveals an endogenous sterol in site-1.

a, Ribbon representation of the complex structure. The CRD and 7-TMs of SMO have been indicated by circles. **b,** The cryo-EM map of ligand. The ligand is shown in sticks and its cryo-EM map is shown at a 0.0102 threshold level. **c,** Structural comparison of the 7-TMs in the SMO^{D384R}, SAG-bound SMO, and 24(*S*),25-EC-bound SMO.

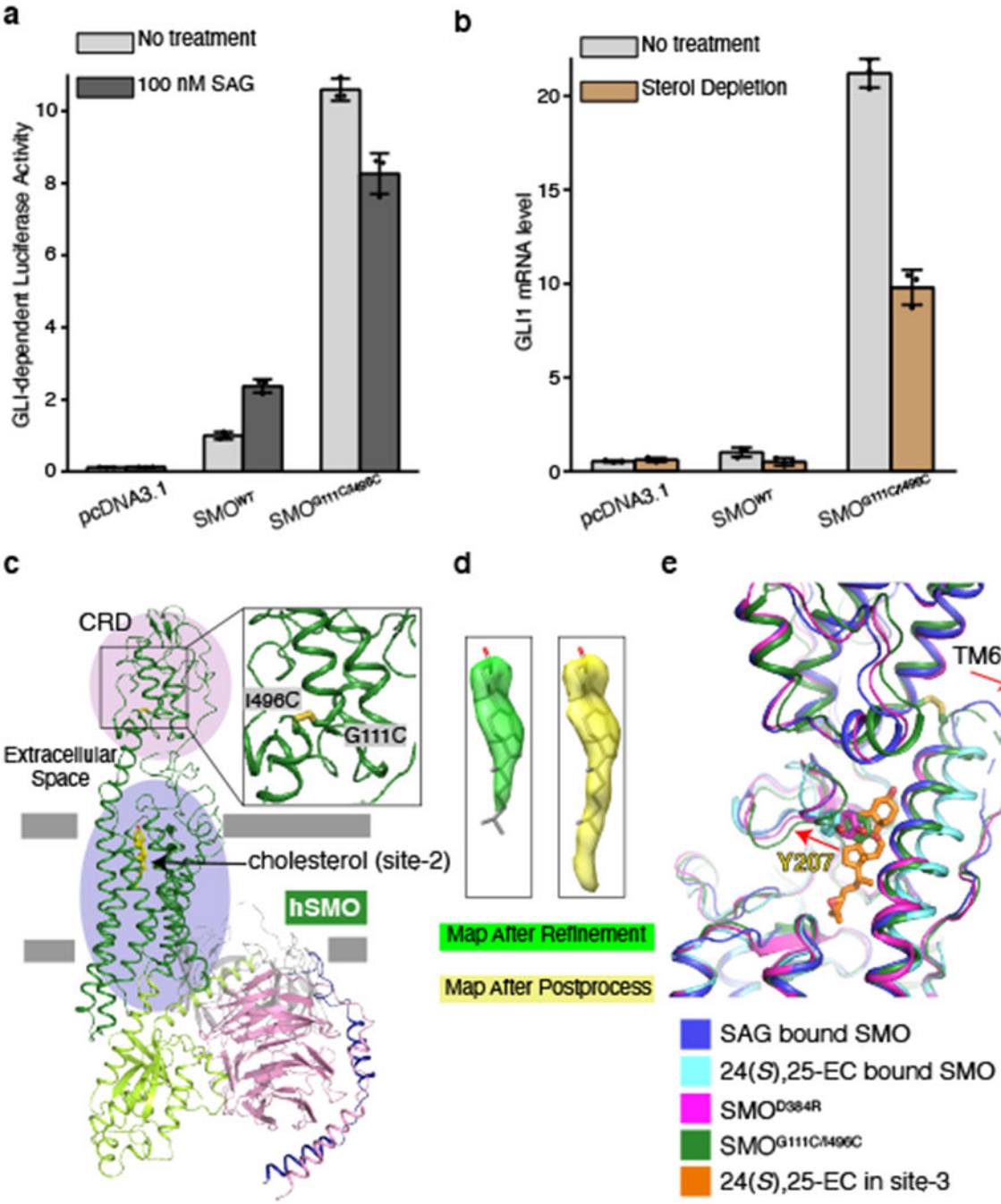

Fig. 5. Structure of SMO$^{G111C/I496C}$–G$_i$ complex suggests site-3 as a sterol gate to control sterol access to CRD.

a, HH signaling in SMO$^{-/-}$ MEFs transfected with pcDNA3.1 and SMO variants. The GLI-dependent luciferase activity was measured. Data are mean ± s.d. (n = 3 biologically independent experiments). **b,** Levels of GLI1 mRNA were used as a metric for HH signaling activity of SMO variants after cholesterol depletion. Data are mean ± s.d. (n = 3 technical repeats). **c,** Ribbon representation of the complex structure. The CRD and 7-TMs of SMO have been indicated by circles. **d,** Cryo-EM map of the ligand. The ligand is shown in sticks

and its maps are shown at 0.00995 (refine) and 0.0126 (postprocessing) threshold levels. **e,** Structural comparison of LD and TM6 in this complex with SMO^{D384R}, SAG-bound SMO, and 24(*S*),25-EC-bound SMO. Residue Y207 and the 24(*S*),25-EC in site-3 are shown as sticks.

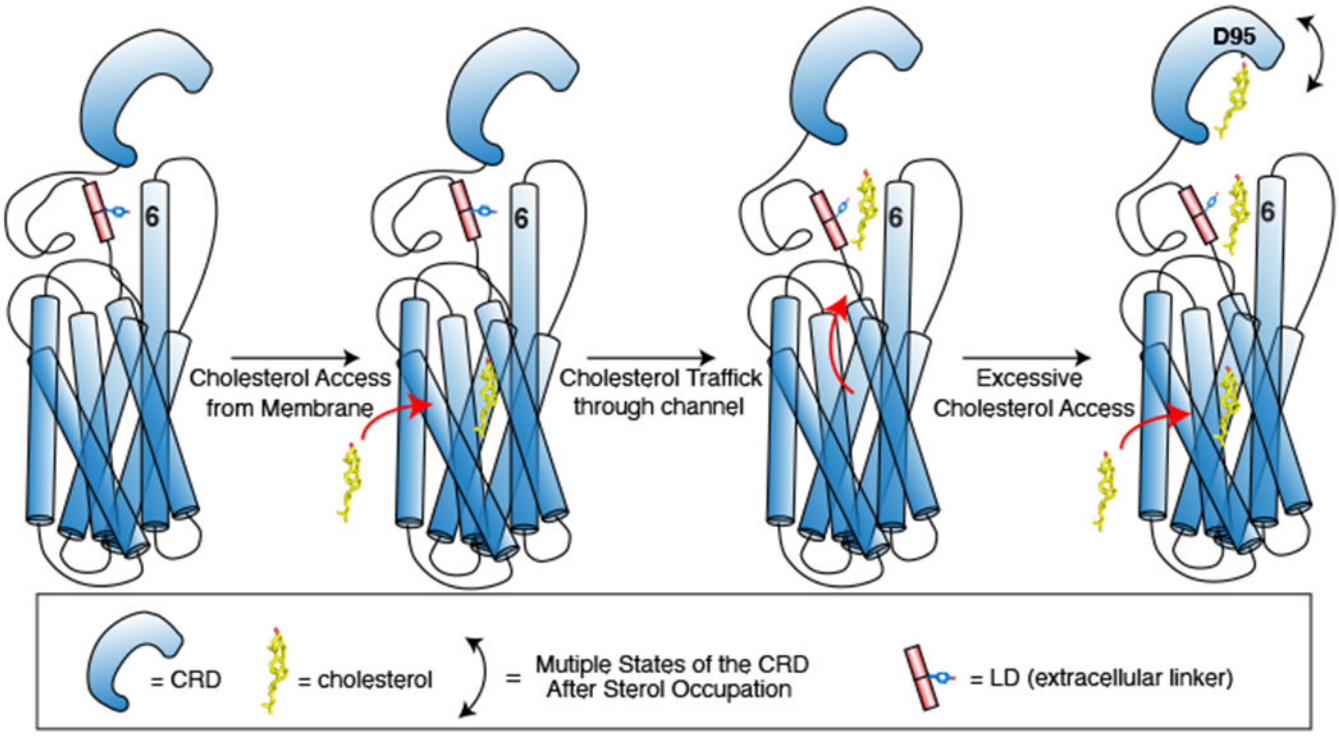

Fig. 6. A working model of the effect of sterols in SMO channel.

When SMO localizes in the intracellular vesicles, not enough free cholesterol occupies all sites in the channel of SMO, so cholesterol may transport through the channel to the CRD. SMO is off in this state. After Hedgehog binds to PTCH1, concentration of free cholesterol would increase on the primary cilium membrane and SMO moves to the cilium. Elevated cholesterol levels may then occupy all sites in the intramolecular channel of SMO, activating SMO for signaling.